JACS
JOURNAL OF THE AMERICAN CHEMICAL SOCIETY

Article

pubs.acs.org/JACS

Dynamics in a Room-Temperature Ionic Liquid from the Cation Perspective: 2D IR Vibrational Echo Spectroscopy

Steven A. Yamada, Heather E. Bailey, Amr Tamimi, Chunya Li, and Michael D. Fayer*

Department of Chemistry Stanford University, Stanford, California 94305, United States

Supporting Information

ABSTRACT: The dynamics of the room-temperature ionic liquid (RTIL) 1-butyl-3-methylimidazolium bis(trifluoromethylsulfonyl)imide ($BmimNTf_2$) were investigated with two-dimensional infrared (2D IR) vibrational echo spectroscopy and polarization selective pump−probe (PSPP) experiments. The CN stretch frequency of a modified $Bmim^+$ cation (2-SeCN-$Bmim^+$), in which a SeCN moiety was substituted onto the C-2 position of the imidazolium ring, was used as a vibrational probe. A major result of the 2D IR experiments is the observation of a long time scale structural spectral diffusion component of 600 ps in addition to short and intermediate time scales similar to those measured for selenocyanate anion ($SeCN^-$) dissolved in $BmimNTf_2$. In contrast to 2-SeCN-$Bmim^+$, $SeCN^-$ samples its inhomogeneous line width nearly an order of magnitude faster than the complete structural randomization time of neat $BmimNTf_2$ liquid (870 ± 20 ps) measured with optical heterodyne-detected optical Kerr effect (OHD-OKE) experiments. The orientational correlation function obtained from PSPP experiments on 2-SeCN-$Bmim^+$ exhibits two periods of restricted angular diffusion (wobbling-in-a-cone) followed by complete orientational randomization on a time scale of 900 ± 20 ps, significantly slower than observed for $SeCN^-$ but identical within experimental error to the complete structural randomization time of $BmimNTf_2$. The experiments indicate that 2-SeCN-$Bmim^+$ is sensitive to local motions of the ionic region that influence the spectral diffusion and reorientation of small, anionic, and neutral molecules as well as significantly slower, longer-range fluctuations that are responsible for complete randomization of the liquid structure.

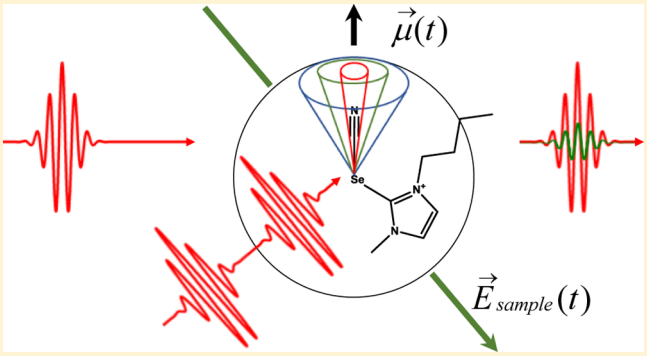

1. INTRODUCTION

Despite their ubiquity and usefulness in chemistry, common solvents such as organic liquids and water often fail to safely and efficiently support processes of technological importance, including carbon dioxide capture and storage, dissolution and processing of biological macromolecules, and proton/ion transport in membrane fuel cells and batteries.[1] Significant research effort is being redirected toward the discovery and characterization of novel solvent systems that meet these particular challenges.

Room-temperature ionic liquids (RTILs), a subgroup of salts that are liquid at temperatures <298 K, have the potential to overcome several problems intrinsic to conventional solvents.[1−3] In contrast to the volatile organic solvent based electrolytes used in traditional lithium-ion batteries, the use of RTILs greatly reduces the risk of fire or explosions owing to their negligible vapor pressures. Their large window of electrochemical stability, on the order of 5−6 V and perhaps higher, means they could eventually serve as electrolytes in supercapacitors and batteries.[4,5] The high solubility of a diversity of molecules and polymers, ranging from CO_2[6] to cellulose (20 wt % in 1-ethyl-3-methylimidazolium acetate)[7] in RTILs suggests that they will play an important role in efforts to mitigate climate change and access alternative sources of renewable energy.

The early observation that RTILs effectively dissolved both polar and nonpolar solutes was perhaps the first indication of their underlying structure.[3] Molecular dynamics (MD) simulations later presented evidence of nanoscale ordering, in which the anions and positively charged head groups of the cation occupied polar regions that are spatially segregated from nonpolar regions formed by the alkyl tails on the cation.[8,9] The size of the domains increased with the length of the alkyl chain on the cation, eventually merging to form an extended bicontinuous phase for very long chains. The structure of such domains, particularly in the 1-alkyl-3-methylimidazolium bis(trifluoromethylsulfonyl)imide ($C_n mimNTf_2$) series, and the threshold chain length at which mesoscopic organization emerges have been the focus of several studies. The consensus view of the most recent experimental[10−13] and MD[14,15] studies is that formation of elongated nonpolar aggregates begins at low values of n, but the percolation of a second continuous nonpolar phase is found to occur for $n \geq 6$.

Received: November 21, 2016
Published: January 18, 2017

DOI: 10.1021/jacs.6b12011
J. Am. Chem. Soc. 2017, 139, 2408−2420

The dynamics in RTILs have been investigated with a variety of time-dependent spectroscopic techniques including optical heterodyne-detected optical Kerr effect (OHD-OKE) spectroscopy,[16−19] time-correlated single photon counting (TCSPC),[20−23] and, more recently, two-dimensional infrared (2D IR) vibrational echo spectroscopy.[24−34] In this study, we investigate the thermal equilibrium dynamics of $BmimNTf_2$ with polarized ultrafast vibrational spectroscopies. The orientational relaxation of two vibrational probe molecules in $BmimNTf_2$ was measured with polarization selective pump−probe (PSPP) experiments. In addition, 2D IR spectroscopy was used to observe the time-dependent structural fluctuations of the RTIL through the frequency fluctuations (spectral diffusion) of the vibrational probe molecules.[35] Since the frequency of an oscillator is sensitive to the surrounding solvent structure, a detailed picture of the dynamic interactions between the liquid and the solute can be obtained by observing its spectral diffusion.

Previous 2D IR studies on RTILs have focused on the dynamics of small molecules that are neutral,[30,32,34] negatively charged,[25,26,31,33] or neutral and hydrogen bonding.[24,27,28] An important observation common to these studies was that the spectral diffusion of the probe was completed on a significantly shorter time scale than the complete structural randomization time of the liquid measured with OHD-OKE spectroscopy. This is noteworthy since spectral diffusion depends on the evolution of the liquid structure, which causes the intermolecular interactions between the probe and RTIL to fluctuate, permitting the probe to sample the frequencies that contribute to its inhomogeneously broadened absorption line shape. It was not intuitively clear why the small probe molecules would undergo complete spectral diffusion (complete sampling of all the frequencies in the inhomogeneous line) substantially faster than the total randomization of the liquid structure. The natural question then is whether slower RTIL dynamics, which are known to exist, can be observed in a 2D IR experiment. Is it possible to obtain a different picture of the amplitudes and time scales of the RTIL dynamics by a vibrational probe molecule that is essentially a component of the RTIL rather than a small solute vibrational probe?

Here we present measurements of the orientational relaxation and spectral diffusion of a newly synthesized vibrational probe based on the structure of the 1-butyl-3-methylimidazolium cation (Figure 1) in the RTIL $BmimNTf_2$ ($C_4mimNTf_2$). A synthetic procedure is introduced in which a SeCN group, whose CN stretch can be probed in PSPP and 2D IR experiments, is substituted onto the C-2 position of the imidazolium ring. The placement of the SeCN as part of the cation headgroup means that it will be located within the polar domains of the liquid. However, the amphiphilic structure of the 2-SeCN-$Bmim^+$ probe implies that its interactions with the liquid are not limited in extent to the polar-regions. The experiments constitute the first 2D IR measurements of RTIL dynamics from the perspective of a positively charged vibrational probe.

A comparison to the dynamics of $SeCN^-$ in $BmimNTf_2$ will made throughout the paper. The orientational dynamics of 2-SeCN-$Bmim^+$ were found to be more restricted and slower relative to those of $SeCN^-$. The multiexponential orientational relaxation decays were analyzed within the framework of a wobbling-in-a-cone model to quantify the angular restrictions and time scales. Within experimental uncertainty, the complete, unrestricted randomization of the transition dipole was found

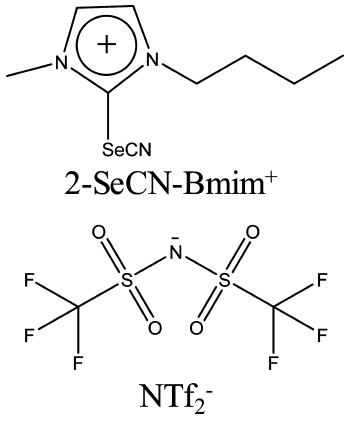

Figure 1. Structures of the vibrational probe 2-SeCN-$Bmim^+$, synthesized from the native ionic liquid cation 1-butyl-3-methylimidazolium ($Bmim^+$), and its counteranion bis(trifluoromethylsulfonyl)-imide (NTf_2^-).

to occur with the same time constant as the complete structural randomization of the liquid, which was extracted from the long time OHD-OKE signal of neat $BmimNTf_2$. The spectral diffusion measurements yielded short and intermediate time scale components that are similar to the spectral diffusion time scales of $SeCN^-$. These components appear to involve local structural fluctuations of the ionic region that completely govern the spectral diffusion of small, anionic and neutral solutes. However, the most significant result is the observation of a third, previously unobserved, long time scale component of the structural spectral diffusion, τ_3 = 600 ps. In contrast to the smaller probe molecules, the final spectral diffusion decay is similar to the time for complete structural randomization of the liquid. The molecular origin of this time scale will be discussed.

2. EXPERIMENTAL PROCEDURES

2.1. Synthesis of 2-SeCN-$BmimNTf_2$ and BmimSeCN. The 2-SeCN-$BmimNTf_2$ salt was synthesized in a multistep procedure (Figure S1). The details of the synthesis and characterization are provided in the Supporting Information. The identity and purity of the solid were confirmed with FT-IR (Figure S2), HPLC-MS (Figure S3), and ^1H NMR (Figure S4). BmimSeCN was prepared according to a previously published synthetic procedure.[36] The Supporting Information contains details on the characterization of the product.

2.2. Sample Preparation and Linear IR Spectroscopy. $BmimNTf_2$ was purchased from IoLiTec Ionic Liquid Technologies Inc., dried under vacuum (∼100 mTorr) at a temperature of 60 °C for 1 week, and stored in a nitrogen glovebox. The water content of the dried IL was assessed with coulometric Karl Fischer titration and found to be below 10 ppm. In the glovebox, the previously synthesized 2-SeCN-$BmimNTf_2$ salt was added to the dry $BmimNTf_2$ gravimetrically at a molar ratio of 1:46 ion pairs to $BmimNTf_2$ ion pairs and mixed overnight. The mixture was filtered through a 0.02 μm inorganic membrane filter (Whatman Anotop). Inspection of the filter showed that roughly $^1/_3$ of the material did not dissolve, which would give a molar ratio of 1:137. Therefore, the initial 1:46 molar ratio should be considered a generous upper bound on the final probe concentration in the liquid. The concentration was kept low to avoid perturbation of the native liquid structure and to ensure that vibrational excitation transfer between neighboring molecules was statistically improbable.

The filtered liquid was sandwiched between two 3 mm thick, 1 in. diameter CaF_2 windows separated by a 250 μm polytetrafluoroethylene (PTFE) ring spacer. The filtration and sample cell assembly were performed in the glovebox to prevent introduction of atmospheric water to the IL. Following assembly, the sample cell was removed from the glovebox and placed in a Thermo Scientific

DOI: 10.1021/jacs.6b12011
J. Am. Chem. Soc. 2017, 139, 2408−2420

Nicolet 6700 Fourier transform infrared (FT-IR) spectrometer, which was purged with CO_2 and H_2O free air. Linear IR spectra were recorded for $BmimNTf_2$ with and without the dissolved probe molecule. The absorption spectrum of the pure IL was subtracted from the spectrum of the probe containing IL to isolate the absorption spectrum of the CN stretch of the 2-SeCN-$Bmim^+$ cation. A peak absorbance of ~0.4 was achieved. For the nonlinear infrared experiments, the sample cell was installed on a sample stage in the 2D IR spectrometer which was purged with H_2O free air and maintained at a constant temperature of 294.8 K. Identical procedures were performed for a sample of BmimSeCN dissolved in $BmimNTf_2$ at 1:100 ion pairs to $BmimNTf_2$ ion pairs.

2.3. Laser System and Optical Setup. A detailed description of the 2D IR spectrometer used in this work can be found elsewhere;[37] a brief version will be presented here. A regenerative amplifier seeded by a Ti:sapphire oscillator outputs 550 μJ pulses centered at 800 nm with a 1 kHz repetition rate. The amplifier output pumps an optical parametric amplifier (OPA) containing a beta barium borate (BBO) crystal, generating near-infrared signal and idler pulses. The signal and idler are difference-frequency mixed in a $AgGaS_2$ crystal, resulting in ~6−7 μJ mid-IR pulses centered at 2108 cm^{-1} (or 2063 cm^{-1}) with ~170 fs full width at half-maximum (fwhm) duration. The mid-IR pulses are split into a strong pump and weaker probe pulse in 92:8 intensity ratio with a ZnSe beam splitter. The strong pump pulse is sent into the input of a mid-IR acousto-optic Fourier-domain pulse-shaper, which provides precise control over the number, amplitude, phase, and temporal delay of the pump pulse(s) that emerge at the output.[37−39] The weak probe pulse enters a mechanical delay stage that sets the time delay between the pump and probe pulses. The pump and probe beams are subsequently focused and overlapped at the sample position. This configuration of the 2D IR spectrometer, referred to as the pump−probe geometry, results in the emission of the vibrational echo signal in the direction of the probe pulse wave-vector.[39] After the sample, the probe/signal is sent into a monochromator acting as a spectrograph and detected on a liquid nitrogen cooled 32-element HgCdTe (MCT) IR array detector.

2.4. Polarization Selective Pump−Probe Experiment. In the PSPP experiment, the pulse shaper was programmed to generate a single pump pulse, which was followed a time t later by the probe pulse, generating the PP signal.[40,41] The delay, t, was incremented with the delay stage. Directly before the sample, the probe polarization was set to horizontal (0° or parallel to the plane of the optical table) with a silicon wire-grid polarizer. The pump polarization was fixed to 45° relative to the probe polarization with a half-wave plate and polarizer. Following the sample, the probe was resolved at +45 and −45°, parallel and perpendicular to the pump polarization respectively, with a polarizer mounted in a computer controlled rotation stage. The parallel, $S_{\parallel}(t)$, and perpendicular, $S_{\perp}(t)$, signals were projected back to horizontal (0°) with a final polarizer before being spectrally resolved and detected. This last step ensured that the detected signals experienced identical grating efficiencies in the spectrograph.

2.5. 2D IR Spectroscopy. In the 2D IR experiment, three pulses interact with the sample, resulting in the emission of the third-order vibrational echo signal in the phase-matched direction.[35,42] In our implementation of the pump−probe geometry, the pulse shaper generates pump pulses 1 and 2, which are separated by a time delay τ, the first coherence period. After a time T_w, the population period, a third probe pulse initiates the second coherence period, t, during which the macroscopic polarization generated in the sample results in emission of the vibrational echo. The phase-matching condition for this geometry results in the emission of the echo collinearly with pulse 3. This is convenient because the probe serves as a phase-locked local oscillator (LO) that heterodynes the emitted echo, amplifying the signal and providing information on its phase.

The following qualitative description is helpful in understanding how the 2D IR pulse sequence measures molecular-scale dynamics. During the first coherence period, pulses 1 and 2 label and store the initial frequencies of the vibrational oscillators. Structural evolution of the solvent during the population period causes the frequency-labeled molecules to sample different frequencies within the inhomogeneously broadened vibrational absorption line. The arrival of pulse 3 begins the second coherence period, during which the final frequencies are read out. A 2D spectrum is constructed by plotting the initial vibrational frequencies along the horizontal axis, ω_τ, and the final frequencies along the vertical axis, ω_m. Detailed structural and dynamical information is contained in the shape of the 2D spectrum, which changes as the waiting time, T_w, is increased. As T_w is increased, the correlation between the initial and final frequencies decreases because structural changes in the liquid cause an increased range of frequencies in the inhomogeneous line to be sampled. The procedures used to transform the measured time domain signals into the frequency domain to generate a 2D spectrum have been thoroughly documented.[35,37] In section 3.4, we discuss how to quantitatively deconvolve the linear absorption spectrum and extract the frequency−frequency correlation function (FFCF) from a T_w series of 2D IR spectra. The FFCF allows us to develop a molecular level picture of the solvent dynamics experienced by a vibrational probe in a RTIL.

The 2D IR experiments were performed with linearly polarized laser pulses by placing polarizers in the pump and probe beam paths. Linearly polarized fields interrogate a subensemble of vibrational probe molecules with a probability proportional to the dot product, $\hat{\varepsilon} \cdot \hat{\mu}$, of the field polarization and transition dipole unit vectors, respectively.[42,43] Parallel and perpendicular polarization configurations, denoted as ⟨XXXX⟩ and ⟨XXYY⟩ respectively, were measured. In the ⟨XXXX⟩ configuration, all pulses were horizontally polarized. In the ⟨XXYY⟩ configuration, the first two pulses were vertically polarized (Y), and the third pulse and the echo detection were horizontal. In addition to the above polarization configurations, the data were acquired using a 4-shot phase cycling scheme discussed in detail previously.[44] The phase cycling was used to remove scatter signals originating from the pump pulses.

2.6. OHD-OKE Spectroscopy. The OHD-OKE experiment is a nonresonant technique in which a linearly polarized pump pulse induces a transient birefringence in the sample. After a time, t, a weaker probe pulse, polarized at 45° relative to the pump, is used to measure the time decay of the birefringence. Any residual birefringence will depolarize the probe pulse, and this depolarization is measured after a crossed polarizer. The resulting time decay is the derivative of the polarizability−polarizability correlation function, which is equivalent to the derivative of the second-order Legendre polynomial orientational correlation function, except at early time during which there are interaction (collision) induced effects.[18,45]

The OHD-OKE experimental setup has been described in detail previously.[18] Briefly, a Ti:sapphire oscillator seeds a 5.4 kHz regenerative amplifier producing pulses with 60 fs to 10 ps fwhm duration (varied according to the time scales being investigated) with a maximum energy of 300 μJ/pulse. The regen output is split into the pump and probe beams used in the experiment. Details of the OKE signal data acquisition were presented in an earlier publication.[18]

3. RESULTS AND DISCUSSION

3.1. Linear IR Spectrum. The normalized, background-subtracted FT-IR spectrum of 2-SeCN-$BmimNTf_2$ dissolved in $BmimNTf_2$ is displayed in Figure 2. Two overlapping peaks are visible. The lower amplitude peak appearing at ~2063 cm^{-1} is assigned to the CN stretch of $SeCN^-$ anion, which is consistent with the absorption spectrum of $SeCN^-$ in $BmimNTf_2$ (inset). The use of KSeCN as a major reagent in the synthesis of the 2-SeCN-$Bmim^+$ probe further supports the assignment. The observed peak absorbance (~0.07), which is directly proportional to the concentration of $SeCN^-$, is a fraction of that used in a previous work[33] (1:200 KSeCN ion pairs per $BmimNTf_2$ ion pairs), ensuring that the IL structure is unperturbed by this small impurity. Thus, the larger, main band in the FT-IR spectrum originates from the CN stretch of the 2-SeCN-$Bmim^+$ cation.

To quantitatively assess the degree of overlap between the $SeCN^-$ and 2-SeCN-$Bmim^+$ bands, the FT-IR spectrum in

DOI: 10.1021/jacs.6b12011
J. Am. Chem. Soc. 2017, 139, 2408−2420

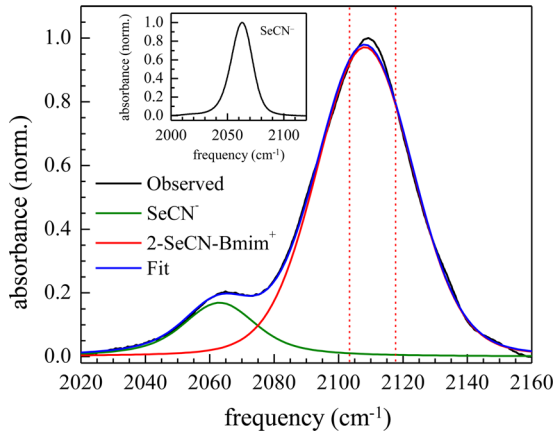

Figure 2. Normalized, background-subtracted FT-IR spectrum (black curve) of 2-SeCN-BmimNTf$_2$ dissolved in BmimNTf$_2$. The FT-IR is fit (blue curve) with the sum of two Voigt line shapes. The small, lower frequency peak, fixed at 2063 cm^{-1} in the fit, is residual SeCN$^-$ (green curve) from KSeCN used in the synthesis of 2-SeCN-Bmim$^+$ (red curve). The dashed, vertical red lines highlight the range of frequencies analyzed in this work. The inset displays the FT-IR spectrum of SeCN$^-$ added as BmimSeCN to BmimNTf$_2$.

Figure 2 was fit with the sum of two Voigt line shape functions, with one peak fixed at the peak position of SeCN$^-$ in BmimNTf$_2$. The fit (blue curve) captures the overall shape of the spectrum but slightly misses the peak of the main 2-SeCN-Bmim$^+$ band. The symmetry of the peak may be distorted by slight errors in the background subtraction or the peak may be intrinsically somewhat asymmetric.[46] In either case, the purpose of the fit is to illustrate, with a reasonable degree of quantitative accuracy, the relative contribution of the two species to the spectrum. It can be seen that in the vicinity of the main peak (red curve) there is essentially no contribution from SeCN$^-$ (green curve). The two red, dashed vertical lines in Figure 2 highlight the range of frequencies analyzed in this work. It is clear that measurements in this region of the spectrum will report solely on the dynamics of the 2-SeCN-Bmim$^+$ probe.

The peak center and fwhm of the CN stretch of 2-SeCN-Bmim$^+$ in BmimNTf$_2$, taken from the original FT-IR (black curve) in Figure 2, were found to be 2109.2 ± 0.5 and 35.1 ± 0.5 cm^{-1} respectively. The line width is significantly broader than for SeCN$^-$ in the same IL. The SeCN$^-$ peak appears at 2063.0 ± 0.5 cm^{-1} with a fwhm of 22.3 ± 0.5 cm^{-1} (inset).

3.2. Isotropic Pump−Probe Decays. In the PSPP experiment, the probe signals parallel, $S_{\parallel}(t)$, and perpendicular, $S_{\perp}(t)$, to the pump polarization (45°) were measured. The measured signals can be expressed as[41,47]

$$S_{\parallel}(t) = P(t)[1 + 0.8C_2(t)] \quad (1)$$

$$S_{\perp}(t) = P(t)[1 - 0.4C_2(t)] \quad (2)$$

where $P(t)$ is the isotropic pump−probe decay and $C_2(t)$ is the second-order Legendre polynomial orientational correlation function of the transition dipole moment given by[40]

$$C_2(t) = \langle P_2[\hat{\mu}(t)\cdot\hat{\mu}(0)]\rangle \quad (3)$$

with P_2 being the second-order Legendre polynomial and $\hat{\mu}(t)$ being the transition dipole moment unit vector at time t. The angle brackets represent an ensemble average. The population decay is obtained by forming the combination

$$P(t) = [S_{\parallel}(t) + 2S_{\perp}(t)]/3 \quad (4)$$

$P(t)$ decays for a range of frequencies (see Figure 2) across the absorption spectrum of 2-SeCN-Bmim$^+$ in BmimNTf$_2$ are shown in Figure 3. The data were analyzed in the range 1.5 ps

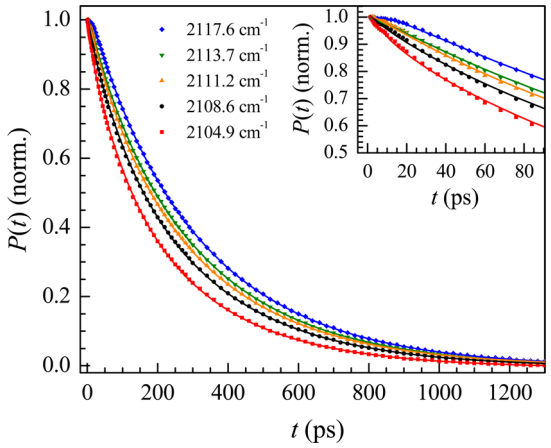

Figure 3. Isotropic pump−probe decays, $P(t)$, at five frequencies (in units of cm^{-1}) across the absorption spectrum of 2-SeCN-Bmim$^+$ in BmimNTf$_2$. The data are normalized to the value at the first time point, 1.5 ps. The solid curves are triexponential fits to the data. The inset magnifies the early time portion of the curves. It is clear from the inset that the data increases at short time on the blue side of the line. The nonexponential behavior comes from spectral diffusion (see text).

to 1.3 ns and normalized to the value at 1.5 ps. A small, constant signal is observed at very long time (1.6 ns) despite the complete decay of the pump−probe signal. This offset is attributed to isotropic heating that results from vibrational relaxation into external bath modes of the IL. Given the negligible amplitude of the long-time signal, its contribution was removed by fitting the data with an offset.

The $P(t)$ signals shown in Figure 3 were found to decay as triexponentials at all frequencies, yet in the case of a single ensemble of vibrational oscillators and uniform excitation across the absorption line (i.e., the excited state population distribution is proportional to the ground state thermal equilibrium distribution), the signal is expected to decay as a single exponential according to the population vibrational lifetime. A previous study on the CN stretch of SeCN$^-$ in D$_2$O[46] also measured multiexponential $P(t)$ decays. The additional time scales were found to originate from nonuniform pumping of the absorption band, as opposed to the presence of multiple subensembles of molecules, each with a distinct lifetime. However, similar to this work, the pump excitation was tuned to the center of the absorption line and had a much larger bandwidth than the absorption spectrum of the vibrational probe, indicating that the pump pulse had uniform intensity across the frequency range under study. Instead, nonuniform pumping was found to originate from the frequency dependence of the transition dipole moment (non-Condon effect) of SeCN$^-$, which increased in strength with decreasing (red-shifted) frequency. The anions with lower oscillator frequencies were excited to a greater extent than those at higher frequencies, producing a nonequilibrium excited state distribution. Spectral diffusion reestablishes the thermal equilibrium population distribution.[46] Population flows from the over pumped red side of the line to the under pumped blue side of the line. The result is that at short times frequencies

DOI: 10.1021/jacs.6b12011
J. Am. Chem. Soc. 2017, 139, 2408−2420

toward the red side show faster decays than the lifetime while frequencies on the blue side show a growth. In general, the components of the spectral diffusion that are faster than the vibrational lifetime will be introduced as either decays or growths in the $P(t)$ signal.

In the main portion of Figure 3, the decays are faster on the red side of the line and slow as the frequency moves to the blue. The inset shows the short time portion of the data. It is clear that at the bluest frequencies the data builds up and then decays, while on the red side of the line there is a faster decay component that then slows at longer time. By subtracting the small band on the red side of the spectrum shown in Figure 2, it was found that the main band is asymmetric with a wing on the red side of the line. This broadening is consistent with a non-Condon effect that would lead to over pumping of the red side of the line. We conclude that the nonexponential decays are caused by spectral diffusion. Therefore, the $P(t)$ data were fit by fixing the first two time constants to the short and intermediate spectral diffusion components measured with the 2D IR experiments (to be discussed in section 3.4), while the third time constant was allowed to vary. This fitting method was previously used to extract the population lifetime in the presence of the non-Condon effect.[27,31,33,46] As can be seen in Figure 3, the fits agree exceedingly well with the data at all times, showing that the first two time scales do indeed originate from the process of spectral diffusion. Using this fitting procedure, the third time constant, the population vibrational lifetime, was found to be 305 ± 2 ps at the center of the main band. The lifetime varies somewhat with frequency, spanning a range of decay times (287−325 ps) moving from red to blue across the range of frequencies analyzed. The time constants as a function of frequency are given in Table S1.

Accounting for the spectral diffusion dynamics in $P(t)$ shows that 2-SeCN-Bmim$^+$ has a single, but frequency-dependent, vibrational lifetime. This supports the conclusion that 2-SeCN-Bmim$^+$ probes the dynamics of a single inhomogeneously broadened distribution of IL environments. Ultimately, the vibrational excitation energy is lost to various accepting modes of the system. The frequency dependence of the transition dipole and vibrational lifetime indicates that the coupling to and/or density of these modes is dependent on the solvent environments encountered at different positions in the absorption spectrum. Simulations of the three-dimensional probability density of NO_3^- around the Emim$^+$ cation in bulk $EmimNO_3$ showed that two anions are located above and below the plane of the imidazolium ring in close proximity to the positive C-2−H bond.[48] The negative oxygen atoms of NO_3^- point toward the bond. Although BmimSeCNNTf$_2$ is a different IL than $EmimNO_3$, the oxygen atoms of NTf_2^- are negatively charged, and despite the SeCN substitution, the C-2 position remains positive. The simulation results suggest that variable interactions between NTf_2^- and the C-2 located SeCN group may give rise to the frequency-dependent lifetime and non-Condon effect evident in $P(t)$. These effects were not previously observed for SeCN$^-$ introduced as KSeCN in BmimNTf$_2$[33] nor in this study as BmimSeCN, which demonstrates that the SeCN moiety of 2-SeCN-Bmim$^+$ experiences different interactions with the IL than SeCN$^-$. This is not surprising given the very different size, structure, and charge of the two probe molecules. The population lifetime of SeCN$^-$ was determined to be 104 ± 2 ps as discussed previously.[33] The data are displayed in Figure S5.

3.3. Orientational Relaxation. In addition to the population lifetime, the orientational relaxation dynamics of 2-SeCN-Bmim$^+$ in BmimNTf$_2$ can be obtained from the PSPP signals. The orientational relaxation dynamics are contained in the correlation function $C_2(t)$, which is recovered from the experiments by calculating the orientational anisotropy[47,49]

$$r(t) = \frac{S_{\parallel}(t) - S_{\perp}(t)}{S_{\parallel}(t) + 2S_{\perp}(t)} = 0.4C_2(t) \quad (5)$$

Equation 5 says that the anisotropy begins at an initial value of 0.4 at t = 0. In an experiment, an initial value of 0.4 is not observed because inertial motions on time scales shorter than the temporal resolution of the experiment, which is fundamentally limited by the pulse durations, cause the transition dipole to quickly sample a portion of the total orientational space. The denominator in eq 5 is the isotropic pump−probe signal of eq 4, which divides out the spectral diffusion and population lifetime dynamics described in section 3.2.

The anisotropy decay of 2-SeCN-Bmim$^+$, averaged over the range of frequencies outlined in Figure 2, is plotted (red squares) in Figure 4 in the range of 1.5−600 ps. The data fits

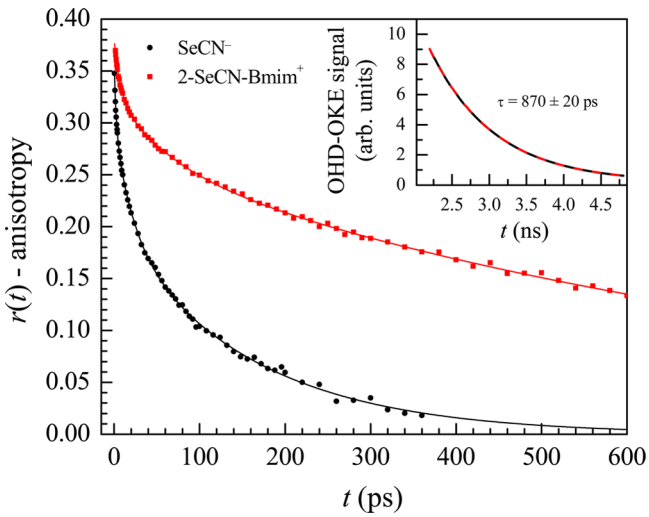

Figure 4. Orientational anisotropy decays, $r(t)$, of 2-SeCN-Bmim$^+$ (red squares) and SeCN$^-$ (black circles) in BmimNTf$_2$ averaged over a range of frequencies, 2104.9−2117.6 cm^{-1} and 2061.3−2071.8 cm^{-1}, respectively, across their absorption lines. The solid curves are triexponential fits to the data. The inset shows the long time OHD-OKE signal (black curve) of neat BmimNTf$_2$, which measures the complete structural randomization time of the liquid, fit (dashed red curve) to a single exponential decay.

well to a triexponential decay (parameters in Table S2). By extrapolating the fit back to t = 0, an initial value of 0.38 was obtained. This value was found to be independent of frequency. The value obtained for SeCN$^-$ was 0.36 and independent of frequency. This is in contrast to the clear frequency dependence observed for the inertial motion of the hydroxyl (OD) stretch of water, methanol, and ethanol in EmimNTf$_2$.[27]

In the case that the orientational relaxation proceeds by free diffusion for the full extent of the anisotropy decay, the orientational correlation function is a single exponential decay

$$C_2(t) = \exp[-6D_m t] \quad (6)$$

DOI: 10.1021/jacs.6b12011
J. Am. Chem. Soc. 2017, 139, 2408−2420

Table 1. Cone Angles, Correlation Times, and Orientational Diffusion Constants from Wobbling-In-A-Cone Analysis[a]

probe	θ_{in} (deg)	θ_{c1} (deg)	θ_{c2} (deg)	θ_{tot} (deg)	τ_{c1} (ps)	τ_{c2} (ps)	τ_{m} (ps)	D_{c1} (10^{-3} ps^{-1})	D_{c2} (10^{-3} ps^{-1})
2-SeCN-Bmim^{+}[b]	10 ± 0.6	18.2 ± 0.6	21.5 ± 0.5	29.7 ± 0.7	7.1 ± 0.9	70 ± 9	900 ± 20	4.0 ± 0.6	0.56 ± 0.08
SeCN^{-}[c]	15.2 ± 0.6	19.9 ± 0.7	29.5 ± 0.5	38 ± 0.8	2.5 ± 0.3	25 ± 2	159 ± 3	14 ± 2	2.9 ± 0.3

[a]Subscripts: in = inertial, c1 = cone 1, c2 = cone 2, tot = total cone, m = free diffusion. [b]Data averaged across frequency range 2104.9−2117.6 cm^{-1}. [c]Data averaged across frequency range 2061.3−2071.8 cm^{-1}.

where D_m is the orientational diffusion constant, and the decay constant is $\tau = 1/6D_m$.[40] The anisotropy decay (Figure 4), however, is clearly not single exponential. The lifetime data demonstrate that the inhomogeneously broadened absorption spectrum is composed of a single ensemble of 2-SeCN-Bmim^{+} cations. A single ensemble eliminates the possibility that the triexponential anisotropy decay arises from three subensembles of 2-SeCN-Bmim^{+} that undergo orientational relaxation with separate diffusion constants.

When orientational relaxation of a single population proceeds in a multiexponential fashion, it is an indication that the motion is restricted relative to the case of simple free diffusion.[27,50] The wobbling-in-a-cone model[49,51,52] provides a framework in which the spatial restrictions and associated correlation times that limit orientational sampling can be quantified. In this model, the transition dipole moment undergoes orientational diffusion within the angular space bounded by a cone of half angle θ_c. Instead of decaying to zero, the orientational correlation function decays to a plateau whose value is the square of a generalized order parameter, Q^2, which is directly related to θ_c. The diffusion constant for diffusive orientational relaxation in a cone can be calculated from θ_c, Q, and τ_c, the wobbling-in-a-cone correlation time. Because the 2-SeCN-Bmim^{+} anisotropy in Figure 4 decays to zero in the long time limit, the final decay involves the unrestricted, complete reorientation of the transition dipole, which occurs by free diffusion. An inertial cone, describing the ultrafast inertial motion, and two diffusive cones, accounting for the short and intermediate exponential decays that precede the complete reorientation, must be included to fit the full extent of the anisotropy. Details of the model and the total $C_2(t)$ (eq S3) used to fit the data are presented in the Supporting Information.

In ILs, the observation of multiple time scales of restricted orientational diffusion is common.[27,30−33] Each diffusive cone represents a limit on the orientational diffusion of the 2-SeCN-Bmim^{+} transition dipole that arises from structural constraints present in the BmimNTf$_2$ IL. Structural fluctuations in the liquid cause these constraints to relax over characteristic correlation time scales, permitting less restricted diffusive motion and more complete angular sampling. The ultrafast inertial motion results in partial angular sampling on a time scale much faster than the diffusive motion. Molecular dynamics simulations of imidazolium ILs find that the velocity autocorrelation function of the cation center-of-mass decays in the subpicosecond regime.[48,53−55] This inertial regime involves librational motions of the cation induced in part by collisions, resulting in a highly limited but rapid decay of $C_2(t)$. Each independent process, whether inertial, restricted diffusion, or free diffusion, relaxes with a distinct correlation time scale.

Table 1 lists several wobbling-in-a-cone parameters determined from the anisotropy decays in Figure 4. It is informative to draw a comparison between the 2-SeCN-Bmim^{+} parameters from the wobbling-in-a-cone analysis and the corresponding parameters obtained for SeCN^{-} in BmimNTf$_2$ (black circles in Figure 4). The anisotropy decays are triexponential in both systems. The general, qualitative trend is that relative to SeCN^{-} the orientational relaxation of 2-SeCN-Bmim^{+} is more restricted (smaller cone angles) and proceeds significantly more slowly (longer correlation times, smaller diffusion constants) across all time scales. Since in the latter case the SeCN group is covalently bound to the significantly larger imidazolium ring of the Bmim^{+} cation, its orientational motion is expected to be increasingly restricted and slowed by structural constraints imposed on the rest of the molecule arising from interactions between the positively charged ring and attached alkyl chains with the ionic regions and nonpolar domains of the IL, respectively. The SeCN^{-}, owing to its small size, less intricate structure, and exclusive localization to the ionic region, encounters steric barriers and interactions which hinder rotation to a much lesser extent. The total randomization of the bulk liquid structure is not required for SeCN^{-} to undergo complete orientational relaxation. Rearrangements of the IL smaller than those required for reorientation of 2-SeCN-Bmim^{+} enable SeCN^{-} to find a path for complete orientational randomization.

The significant slowing of the complete orientational relaxation time, τ_m, observed when the vibrational probe is changed from SeCN^{-} to 2-SeCN-Bmim^{+} (Table 1) is perhaps unsurprising considering the difference in size of the two solutes. Under constant temperature and viscosity, hydrodynamics predicts that large solutes reorient more slowly than small solutes, unless the shape of the solutes or their interactions with the liquid differ significantly.[56−58] The bulk viscosity of BmimNTf$_2$ is unaltered by the very low probe concentrations used in the experiments. It was previously determined that the complete orientational relaxation time measured for SeCN^{-} in BmimNTf$_2$ matched the hydrodynamic prediction under slip boundary conditions.[33] We performed a calculation to determine whether hydrodynamics also accurately predicts τ_m for 2-SeCN-Bmim^{+}. Stick boundary conditions, which tend to hold when the solute is much larger than the solvent, involve rotation of the solvent along with the solute. Considering the similarity in size of 2-SeCN-Bmim^{+} and the surrounding solvent ions, we expected slip rather than stick boundary conditions to hold. In the limit of slip boundary conditions, the tangential component of stress on the rotating solute vanishes;[56,57,59] rather, the friction arises from the need for displacement of solvent molecules when the solute rotates. To calculate the orientational diffusion constant under slip boundary conditions, we used a modified Debye−Stokes−Einstein (DSE) equation[56−58] given by

$$D = \frac{k_B T}{\eta V_{eff}\, \lambda(\rho)} \tag{7}$$

where η is the dynamic viscosity, V_{eff} is the spheroidal volume of the molecule, and $\lambda(\rho)$ is a dimensionless friction coefficient that is a function of the ratio, ρ, of the short to long semiaxes of the spheroid. The details of the calculation can be found in the Supporting Information. The dimensionless friction coefficients

DOI: 10.1021/jacs.6b12011
J. Am. Chem. Soc. 2017, 139, 2408−2420

have been previously tabulated as a function of ρ.[58] Using eqs S4 and 7, we estimated the complete orientational relaxation time to be 790 and 960 ps using the nearest tabulated and interpolated values of the friction coefficient, respectively. The experimentally measured orientational diffusion time of 900 ± 20 ps is in good agreement with the hydrodynamic prediction under slip boundary conditions. It is within the variation due to small changes in the axis ratio ρ. We conclude that the main source of friction impeding the complete diffusive orientational relaxation of 2-SeCN-Bmim$^+$ is the displacement of surrounding ions of the liquid as the molecule rotates.

The inset to Figure 4 shows the long time (2200−4800 ps) OHD-OKE signal (black curve) of neat BmimNTf$_2$ fit to a single exponential decay (red dashed curve). As mentioned in section 2.6, the longtime OHD-OKE signal is the derivative of the polarizability−polarizability correlation function of the liquid. The decay constant, τ = 870 ± 20 ps, gives the time for complete structural randomization of the liquid. (Improved data quality and fitting procedures resulted in the value reported here which is somewhat faster than a previous report.)[33] Within experimental uncertainty, this is the same as the complete orientational relaxation time of the vibrational probe 2-SeCN-Bmim$^+$. The result demonstrates that the complete orientational randomization of the probe tracks that of the entire IL. The agreement between the PSPP and OHD-OKE experiments supports the notion that an accurate picture of the neat IL dynamics can be obtained if the interactions between the vibrational probe and the liquid mirror those between the native cation and the liquid.

Several groups have simulated the orientational correlation function of C$_n$mim$^+$ cations in ILs with variable anions at elevated and room temperature.[48,53−55] The Bmim$^+$ orientational relaxation was found to occur on a time scale of several hundred picoseconds in BmimNTf$_2$.[54] Interestingly, the reorientation time depended on the particular vector chosen in the cation molecular frame, that is, the reorientation was spatially anisotropic, in agreement with other works.[48,53] At 298 K, reorientation times of 300 ps or 1 ns were obtained for Bmim$^+$ in BmimNTf$_2$ depending on whether the chosen vector pointed normal to the ring or along the long axis of the cation, respectively.[54] The superior agreement between the results herein and the latter number may indicate that the experimental signals are dominated by the orientational relaxation of the long axis of 2-SeCN-Bmim$^+$ and Bmim$^+$.

3.4. Spectral Diffusion. 2D IR spectroscopy provides a quantitative measure of spectral diffusion, which captures the amplitudes and time scales of the loss of correlation between initial and final oscillator frequencies. The correlation decays as an increasing number of solvent structures responsible for inhomogeneous broadening are sampled. In an experiment, a series of 2D spectra are acquired as a function of increasing waiting time, T_w. The change in shape of the 2D spectrum with T_w reports on the time-dependent structural evolution of the system.

In this work, the center line slope (CLS) method[60,61] is used to extract the time dependence of the spectral diffusion from a T_w series of 2D spectra. The CLS ω_m method[61] (subsequently referred to as CLS) is particularly reliable in the presence of line shape distortions. In this version of the method, slices through the 2D spectrum are taken parallel to the ω_m axis for a range of ω_τ in the vicinity of the peak. Plotting the maxima of the slices on the 2D spectrum forms a line whose slope is the CLS. Within certain approximations, the CLS decay is equal to the T_w-dependent, normalized frequency−frequency correlation function (FFCF). The FFCF is the joint probability that an oscillator with an initial frequency will have the same frequency at a time t later, averaged over all initial frequencies in the inhomogeneous spectral distribution. The FFCF, which quantifies the amplitudes and time scales of the spectral diffusion, was modeled with the form

$$C(t) = \langle \delta\omega(t)\, \delta\omega(0)\rangle = \sum_i \Delta_i^2 \exp[-t/\tau_i] \tag{8}$$

where $\delta\omega(t) = \omega(t) - \langle\omega\rangle$ is the fluctuation of the instantaneous frequency, $\omega(t)$, from the average frequency, $\langle\omega\rangle$. Δ_i and τ_i which appear in eq 8 are the frequency fluctuation amplitude and time constant, respectively, of the ith component. A component of the FFCF is motionally narrowed, and a source of homogeneous broadening in the absorption line if $\tau\Delta \ll 1$. When a component is motionally narrowed, it is not possible to determine Δ and τ separately. The motionally narrowed contribution to the absorption spectrum has a pure dephasing line width given by $\Gamma^* = \Delta^2\tau/\pi = 1/\pi T_2^*$, where T_2^* is the pure dephasing time. However, the observed homogeneous dephasing time, T_2, also depends on the vibrational lifetime and transition dipole orientational relaxation

$$\frac{1}{T_2} = \frac{1}{T_2^*} + \frac{1}{2T_1} + \frac{1}{3T_{or}} \tag{9}$$

where T_1 and T_{or} are the vibrational lifetime and orientational relaxation time, respectively. The total homogeneous line width is $\Gamma = 1/\pi T_2$. The total dephasing time, T_2, and the absolute fluctuation amplitudes, Δ_i, in frequency units, are calculated by simultaneously fitting the CLS decay and the linear absorption spectrum,[60] providing the complete FFCF of eq 8. In this manner, 2D IR combined with the CLS method determines the absolute contribution of homogeneous and inhomogeneous broadening to the total line width.

As discussed in section 2.5, 2D IR experiments were performed in ⟨XXXX⟩ (parallel) and ⟨XXYY⟩ (perpendicular) polarization configurations. It was recently observed that the CLS decays obtained with these two polarization pathways are not necessarily the same, demonstrating that in certain cases isotropic structural fluctuations of the sample medium do not entirely determine the frequency fluctuations of the vibrational probe.[28] The difference in the parallel and perpendicular decay curves was addressed by modeling the interaction of the vibrational transition dipole with its surroundings as a vector frequency fluctuation through a first-order Stark coupling to the electric field produced by the sample.[28,43] When the field varies on a similar time scale, or slowly, relative to the orientational relaxation time scales of the probe molecule, frequency fluctuations occur due to the probe rotation via changes in the dot product of the electric field and the difference in the dipole moment of the probe vibration in the ground and first vibrational excited state. The dipole moment difference will be along the CN bond direction. Therefore, reorientation of the probe molecule contributes to spectral diffusion and gives rise to different CLS decays for ⟨XXXX⟩ and ⟨XXYY⟩ polarization configurations.[28,43] This phenomenon is referred to as reorientation-induced spectral diffusion (RISD), in contrast to structural spectral diffusion (SSD), which arises solely from structural evolution of the liquid. In general, we are interested in measuring SSD. Analytical expressions are available for the RISD contribution to the polarization weighted FFCF (PW-

DOI: 10.1021/jacs.6b12011
J. Am. Chem. Soc. 2017, 139, 2408−2420

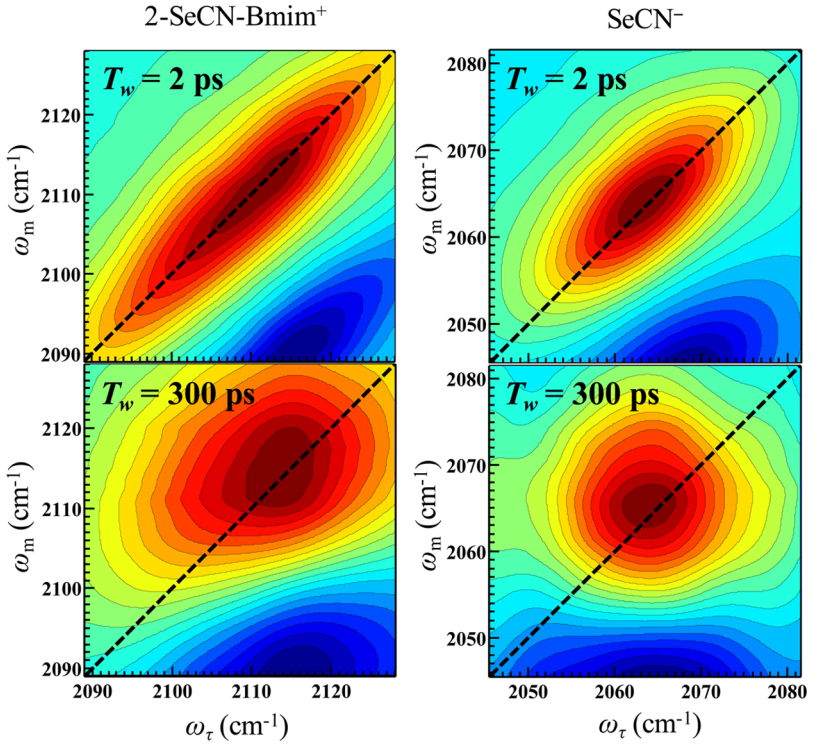

Figure 5. Isotropic 2D IR spectra of 2-SeCN-Bmim$^+$ and SeCN$^-$ in BmimNTf$_2$ at T_w = 2 and 300 ps. The black, dashed line is the diagonal. The 2D spectrum, which is elongated along the diagonal at short T_w, becomes round at longer T_w due to spectral diffusion.

FFCF), and the SSD and RISD contribution were shown to factor

$$C_v^p(t) = F(t)\, R_p(t) \tag{10}$$

where $F(t)$ is the SSD decay and $R_p(t)$ is the RISD factor, which contains the polarization dependence of the PW-FFCF, $C_v^p(t)$. The normalized RISD factors are given by[28,43]

$$R_{para}(t) = \frac{3}{25}\left[\frac{11C_1(t) + 4C_3(t)}{1 + 0.8C_2(t)}\right] \tag{11a}$$

$$R_{perp}(t) = \frac{3}{25}\left[\frac{7C_1(t) - 2C_3(t)}{1 - 0.4C_2(t)}\right] \tag{11b}$$

$$R_{iso}(t) = C_1(t) \tag{11c}$$

for ⟨XXXX⟩, ⟨XXYY⟩, and isotropic (⟨XXXX⟩ + 2⟨XXYY⟩) polarization configurations, respectively. $C_l(t)$ in eqs 11 are the lth order Legendre polynomial orientational correlation functions of the transition dipole unit vector. Polarization selective pump−probe experiments measure the second-order correlation function, $C_2(t)$.[40,41] All other orders of $C_l(t)$ can be calculated from knowledge of $C_2(t)$, whether the orientational relaxation occurs by free diffusion, in which the decay is single exponential for all orders (eq 6), or a restricted manner of orientational relaxation, such as in the wobbling-in-a-cone model.[43] Thus, PSPP experiments permit the complete calculation of the RISD factors $R_p(t)$, which appear in eq 10, such that the only adjustable parameters in the fit to the experimental CLS are contained in $F(t)$, the SSD factor of interest.

2D IR spectra were measured for 2-SeCN-Bmim$^+$ and SeCN$^-$ in BmimNTf$_2$ for T_w ranging from 1.5 to 540 ps and 0.5 to 300 ps, respectively. Figure 5 displays 2D IR spectra for the two systems at the waiting times 2 ps (top panel) and 300 ps (bottom panel). The red, positive-going band that appears on the diagonal (dashed line) arises from the 0−1 vibrational transition. The blue, negative-going band (only partially shown) below the 0−1 band comes from the 1−2 transition. This band is shifted to lower frequency along the ω_m axis by the vibrational anharmonicity. The information on the spectral diffusion is obtained from analysis of the 0−1 band. The 0−1 transition, which reports on the thermal equilibrium dynamics,[60,61] was used in the CLS analysis. As T_w is increased, spectral diffusion causes the band to become less elongated along the diagonal and increasingly round as can be seen in Figure 5.

The CLS decay data for the ⟨XXXX⟩, ⟨XXYY⟩, and isotropic polarization configurations are shown in Figure 6A for 2-SeCN-Bmim$^+$. The isotropic decay also contains the influence of RISD (see eq 11c). The isotropic decay is what would be calculated in an MD simulation, as simulations generally do not include the polarized radiation fields that give rise to the data. The isotropic CLS was obtained after reconstructing the isotropic 2D IR spectra by forming the combination ⟨XXXX⟩ + 2⟨XXYY⟩ and then proceeding with the CLS method. The parallel and perpendicular spectra were properly scaled using the PSPP data as has been described previously.[30]

Figure 6A shows that a relatively small difference is observed in the recorded CLS decays across the three polarization configurations. The difference indicates that RISD has at most a small influence on the frequency fluctuations of 2-SeCN-Bmim$^+$ in BmimNTf$_2$. The CLS decays all begin around a value of 0.88 and are essentially identical at times <25 ps. To begin the analysis, RISD was neglected and the data were fit (Figure 6A) with triexponential decays in which all three time constants were shared. Table 2 displays the amplitudes and time

DOI: 10.1021/jacs.6b12011
J. Am. Chem. Soc. 2017, 139, 2408−2420

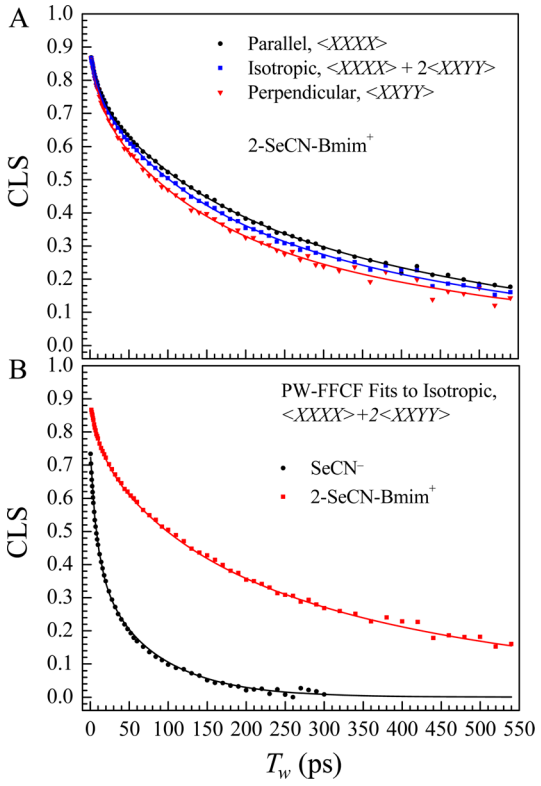

Figure 6. (a) Parallel, isotropic, and perpendicular CLS decays for 2-SeCN-Bmim$^+$ in BmimNTf$_2$. The solid curves are triexponential fits to the data. (b) Isotropic CLS decays for 2-SeCN-Bmim$^+$ (red squares) and SeCN$^-$ (black circles) in BmimNTf$_2$ fit (solid curves) to the PW-FFCF of eq 10, using the RISD factor in eq 11c constructed from the wobbling-in-a-cone parameters in Table 1.

constants of the triexponential fits to the CLS curves in Figure 6A.

To obtain the SSD parameters, all three data sets shown in Figure 6A were fit simultaneously with $F(t)$ appearing in eq 10 modeled as a triexponential decay. The appropriate RISD factor from eqs 11 was used. As stated above, there are no adjustable parameters in the RISD factors. The purpose of the analysis is to separate the isotropic SSD factor, which identically influences all polarization configurations, from the RISD contribution. The isotropic CLS data for 2-SeCN-Bmim$^+$ from Figure 6A are reproduced in Figure 6B (red squares) with the fit (red curve) using the RISD factor in eq 11c. The SSD fit parameters are shown in Table 2. Within the error, the amplitudes and time constants are essentially identical to the corresponding parameters obtained from the fits to a simple triexponential decay (Table 2, rows 2−4). Ignoring the error bars, the values of the time constants obtained in the SSD decay are slightly longer, which is consistent with removing a small RISD contribution to the CLS decay. RISD is not very significant in this system, in contrast to some of the RTIL systems studied previously,[28,30−33] because the orientational dynamics of the vibrational probe, 2-SeCN-Bmim$^+$, are slow. The dominant term in the RISD equations (eqs 11) is $C_1(t)$. For a single exponential decay, which occurs here at long time (free diffusion regime) in the anisotropy data, $C_1(t)$ is a factor of 3 slower than $C_2(t)$. Also, τ_m = 900 ps (see Table 1), which means that the RISD contribution from the complete orientational randomization occurs on a time scale (∼2700 ps) that is so much slower than the SSD that it has little effect. The two wobbling components (Table 1), while on time scales that can influence the CLS, have small amplitudes, and therefore do not contribute much to the total spectral diffusion.

The isotropic CLS data for SeCN$^-$ are also shown in Figure 6B (black circles) with the corresponding fit (black curve) to eq 10. Ignoring RISD, the CLS decays across all polarization configurations for SeCN$^-$ are triexponential (Figure S6). The triexponential fit parameters are provided in Table 2. The difference between the fits, particularly with regard to the time scales, across-polarization configurations indicates that RISD influences the CLS decays to a larger extent for the SeCN$^-$ system, which reorients much more rapidly compared to 2-SeCN-Bmim$^+$ (Table 1). From Figure 6B it is very clear that the spectral diffusion of SeCN$^-$ in BmimNTf$_2$ is significantly faster than that of the cation, 2-SeCN-Bmim$^+$. Again, the parallel and perpendicular data were fit simultaneously with the isotropic data to a single $F(t)$. In the case of SeCN$^-$, $F(t)$ was found to be biexponential in contrast to the triexponential form found for 2-SeCN-Bmim$^+$. No improvement of the fit could be obtained by including additional exponential terms, and the biexponential model was supported by the Akaike information criterion (AIC).[62] The SSD fit parameters for SeCN$^-$ are provided in the final row of Table 2.

The total dephasing time, homogeneous line width, frequency fluctuation amplitudes, and decay time constants for the FFCFs extracted from the isotropic CLS decays (Figure 6B) are given in Table 3. The FFCFs extracted from MD simulations of these systems should correspond most closely to those provided in Table 3, which include the influence of RISD and do not require polarization-weighting in the ensemble averaging. Each frequency fluctuation amplitude, Δ_i, is the standard deviation of the Gaussian line shape associated with

Table 2. CLS and SSD Fit Parameters for 2-SeCN-Bmim$^+$ and SeCN$^-$ in BmimNTf$_2$[a]

probe		A_1	τ_1 (ps)	A_2	τ_2 (ps)	A_3	τ_3 (ps)
2-SeCN-Bmim$^+$[b]	parallel	0.12 ± 0.01	12 ± 2	0.25 ± 0.04	110 ± 20	0.52 ± 0.04	490 ± 40
	isotropic	0.12 ± 0.01	12 ± 2	0.29 ± 0.04	110 ± 20	0.47 ± 0.04	490 ± 40
	perpendicular	0.15 ± 0.02	12 ± 2	0.33 ± 0.03	110 ± 20	0.41 ± 0.04	490 ± 40
	$F(t)$[c]	0.09 ± 0.02	15 ± 6	0.3 ± 0.1	130 ± 50	0.5 ± 0.1	600 ± 100
SeCN$^-$	parallel	0.17 ± 0.02	4.6 ± 0.7	0.29 ± 0.02	27 ± 4	0.30 ± 0.03	114 ± 7
	isotropic	0.14 ± 0.03	3.3 ± 0.7	0.27 ± 0.02	16 ± 3	0.35 ± 0.02	80 ± 3
	perpendicular	0.15 ± 0.03	2.5 ± 0.5	0.29 ± 0.02	13 ± 2	0.33 ± 0.02	69 ± 3
	$F(t)$[c]	0.30 ± 0.01	10.2 ± 0.9	0.47 ± 0.02	94 ± 4		

[a] A_i and τ_i are the amplitudes and time constants of the ith component of the fits to the CLS data, respectively. [b] τ_i were shared across all polarization configurations. [c] SSD parameters obtained from a simultaneous fit of eq 10, using eqs 11 and the PSPP data, to the parallel, perpendicular, and isotropic CLS decays.

DOI: 10.1021/jacs.6b12011
J. Am. Chem. Soc. 2017, 139, 2408−2420

Table 3. FFCF Parameters from Isotropic CLS[a]

probe	T_2 (ps)	Γ (cm^{-1})	Δ_1 (cm^{-1})	τ_1 (ps)	Δ_2 (cm^{-1})	τ_2 (ps)	Δ_3 (cm^{-1})	τ_3 (ps)
2-SeCN-Bmim$^+$[b]	1.6 ± 0.8	7 ± 3	4.9 ± 0.3	12 ± 2	7.7 ± 0.5	110 ± 20	9.8 ± 0.6	490 ± 40
$SeCN^-$[c]	1.8 ± 0.4	5.8 ± 1	3.5 ± 0.1	3.3 ± 0.7	4.8 ± 0.2	16 ± 3	5.5 ± 0.2	80 ± 3

[a] T_2 and Γ are the total dephasing time and homogeneous line width, respectively. The Δ_i and τ_i are the absolute frequency fluctuation amplitude and time constant of the ith component, respectively. [b] RISD contribution included but negligible. [c] RISD contribution included.

Table 4. Comparison of Vibrational Probe Spectral Diffusion Time Constants in $BmimNTf_2$

probe	polarization	τ_1 (ps)	τ_2 (ps)	τ_3 (ps)
BmimSCN[26a]	parallel	5 ± 2	58 ± 13	
BmimSeCN	isotropic	10.2 ± 0.9	94 ± 4	
2-SeCN-$BmimNTf_2$[b]	isotropic	12 ± 2	110 ± 20	490 ± 40

[a] RISD contribution included. (If removed, the time scales will become longer, improving the agreement with the other probes.). [b] RISD contribution included but negligible.

the ith component of the total inhomogeneous line shape. The standard deviation of the total inhomogeneous line width is given by the convolution of the Gaussian components, $\Delta_{total} = (\Delta_1^2 + \Delta_2^2 + \Delta_3^2)^{1/2}$, and the fwhm of the total inhomogeneous line shape is $2.35\Delta_{total}$. The linear absorption line shape is then given by the convolution of the homogeneous and total inhomogeneous line shapes.

3.5. Structural Dynamics in $BmimNTf_2$. Spectral diffusion in $BmimNTf_2$ has previously been measured using small vibrational probes.[25−28,30−34] The vibrational probes employed were either neutral, in the case of CO_2,[30,32,34] or negatively charged, in the case of SCN^-[25,26] and $SeCN^-$[31,33] anions. Unlike previous investigations, the 2-SeCN-Bmim$^+$ probe used in this work is a derivative of the native IL cation and is therefore significantly larger than previously studied probes, more comparable in structure to a constituent ion of the IL, and positively charged. In the earlier studies, the data indicated that the probe molecules were localized in the polar regions of the ILs. The SeCN functionality of 2-SeCN-Bmim$^+$, which resides on the C-2 position of the positively charged imidazolium ring, will also interact with the polar domains.

The influence of RISD on the measured CLS was observed and addressed in the cases of CO_2 and $SeCN^-$. However, because CO_2 is symmetric to inversion, it does not have a difference dipole between its ground (n = 0) and first excited state (n = 1), causing the first-order Stark coupling between the vibrational transition frequency and the sample electric field to vanish. The Stark effect was therefore expanded to second-order in the field,[30] the coupling instead depending on the difference polarizability tensor between the n = 0 and 1 states. The differences in the data analysis do not make direct comparison with the charged polar probes straightforward. The most important aspect of the CO_2 results in the context of the current study is that like the small charged probes complete spectral diffusion occurs on a relatively short time scale, much shorter than the time for the complete randomization of the $BmimNTf_2$ liquid structure.[30,32,34]

The spectral diffusion time constants obtained with the vibrational probes SCN^-,[26] $SeCN^-$, and 2-SeCN-Bmim$^+$ in $BmimNTf_2$ are given in Table 4. The SCN^- data were acquired in ⟨XXXX⟩ configuration and did not take RISD into account.[26] The remaining isotropic data were taken in this work and have the RISD contribution removed. Within experimental error, the short spectral diffusion time scale, τ_1, is identical for $SeCN^-$ and 2-SeCN-Bmim$^+$. Previously, the invariance of τ_1 as measured using $SeCN^-$ (added as KSeCN) as a function of the RTIL chain length in the $C_nmimNTf_2$ IL series, where n = 2, 4, 6, and 10, indicated that the structural motions of the liquid related to this correlation time scale were relatively insensitive to the onset and formation of distinct polar and nonpolar domains of mesoscopic length scales by n = 10.[33] The motions that give rise to τ_1 were assigned to fast fluctuations involving the imidazolium ring that were minimally influenced by the alkyl chain ordering in the nearby nonpolar domains. The appearance of an identical time scale in the spectral diffusion of $SeCN^-$ (added as BmimSeCN) and 2-SeCN-Bmim$^+$ indicates that the CN frequency of 2-SeCN-Bmim$^+$ is sensitive to the fast, restricted motions of the imidazolium rings, which may include the 2-SeCN-Bmim$^+$ itself and the associated anions.

The longest time scale components, τ_2, measured for SCN^- and $SeCN^-$ are very similar to each other and to the intermediate component (also denoted τ_2) of the 2-SeCN-Bmim$^+$ spectral diffusion (Table 4). The values for $SeCN^-$ and 2-SeCN-Bmim$^+$ are within each other's error bars. The reasonable correspondence of the τ_2 values for the three probes suggests that they arise from related structural motions of the liquid. In the previous $SeCN^-$ study, as the imidazolium alkyl chain was lengthened, a significant slowing of τ_2 was observed.[33] Based on the observed chain length dependence, the fluctuations giving rise to τ_2 were taken to originate from longer length scale motions than those responsible for τ_1 and required non-negligible rearrangement of the alkyl chains of the nonpolar regions. The τ_2 for 2-SeCN-Bmim$^+$ may be slightly slower than for the smaller probes because it is sensitive to a broader range of motions, likely involving the alkyl regions, with slow dynamics (note that Δ_2 is larger for 2-SeCN-Bmim$^+$ than $SeCN^-$ in Table 3).

The most significant result of the spectral diffusion measurements is the observation of a third, considerably longer correlation time τ_3 = 490 ± 40 ps for 2-SeCN-Bmim$^+$ (Tables 3 and 4), which is not observed for SCN^- and $SeCN^-$, as well as other small probes, including CO_2,[30,32,34] H_2O, methanol, and ethanol,[27] not discussed here. The long time component, which is the time scale on which 2-SeCN-Bmim$^+$ completely samples its inhomogeneous line, is the largest amplitude component of the spectral diffusion as can be seen in Table 3 by comparing the Δ_i.

Previous 2D IR investigations of ILs using small vibrational probes[24,27,30−33] noted that spectral diffusion proceeded on a significantly faster time scale than the complete structural randomization time of the ILs measured with OHD-OKE. The

DOI: 10.1021/jacs.6b12011
J. Am. Chem. Soc. 2017, 139, 2408−2420

smaller probes were able to completely sample the solvent structures contributing to the inhomogeneous broadening well before the total rearrangement of the IL. These results demonstrate that the intermolecular interactions that give rise to the inhomogeneous broadening, and the dynamics that sample the structures that result in complete spectral diffusion do not involve all structural degrees of freedom of the IL. This is not the situation for the present probe, 2-SeCN-Bmim$^+$. As discussed in section 3.3, the OHD-OKE experiment on neat BmimNTf$_2$ measured a complete structural randomization time of 870 ± 20 ps, which is within error of the 900 ± 20 ps complete orientational relaxation time, τ_m, measured for 2-SeCN-Bmim$^+$ in BmimNTf$_2$. Thus, the long time scale component of the structural spectral diffusion, at most 600 ps (Table 2), is near the time for complete randomization of the liquid. As a comparison, the longest component of the spectral diffusion for SeCN$^-$ (94 ± 4 ps) is approximately an order of magnitude faster than the complete structural randomization time of BmimNTf$_2$.

The 2-SeCN-Bmim$^+$ orientational relaxation and FFCF decay on three distinct time scales. The similarity between the slowest SSD time scale and the complete randomization of the liquid is particularly noteworthy. The apparent correspondence raises the question as to whether the spectral diffusion and the bulk liquid orientational relaxation dynamics are influenced by related, or coupled, structural motions of the vibrational probe molecule and the solvating ions of the liquid. For example, in bulk water (HOD in H_2O), the longest components of the orientational relaxation and spectral diffusion, 2.6 and 1.7 ps, respectively, are close in magnitude.[63] Whereas the reorientation is dominated by large angle jumps (~60°) of individual molecules,[64−66] the FFCF decay originates from multiple-body reorganization dynamics of the extended hydrogen bond network.[67,68] Randomization of the hydrogen bond network necessarily includes reorientation of constituent water molecules, in addition to a multitude of processes that lead to fluctuations in the collective structure. Thus, although $C_2(t)$ and the FFCF are fundamentally different correlation functions, similar time scales can be observed in the case that they are sensitive to the same underlying physical motion. In analogy to water, we find that the long time scale component of the spectral diffusion and the complete orientational randomization time of BmimNTf$_2$ (~600 ps vs ~900 ps) are similar in magnitude. Comparing the orientational relaxation to the OHD-OKE measurements showed that 2-SeCN-Bmim$^+$ randomizes its orientation on a time scale consistent with the complete randomization of the IL structure. Therefore, the results indicate that the final component of the SSD reports on the collective reorganization of a complex network of interacting Bmim$^+$ and NTf$_2^-$ ions and the associated polar and nonpolar domains (alkyl chains). The results also show that the inhomogeneous line width of 2-SeCN-Bmim$^+$ has contributions from essentially all the degrees of freedom of the IL in contrast to the small vibrational probes, which have contributions to their inhomogeneous lines that involve a subset of degrees of freedom that randomize faster than the total liquid.

4. CONCLUDING REMARKS

Room-temperature ionic liquids are complex systems with mesoscale structuring. Using ultrafast nonlinear IR methods, a great deal has been learned about the dynamics of RTILs by studying vibrational probe solutes in the liquids. The IR experiments provide information on the dynamics of the liquid structure and intermolecular interactions that influence the probe molecule. Generally, the vibrational probes have been small molecules or ions such as water,[27] CO_2,[30,32,34] and SeCN$^-$.[31,33] The chemical nature of the probe will dictate whether it principally interacts with the larger cations or anions that make up the IL, as well as the nature and strength of its intermolecular interactions with the liquid. Nonetheless, all probes are influenced by complex interactions and dynamics involving both cations and anions that make up the liquid.

The two informative IR observables are orientational relaxation, measured with PSPP experiments, and spectral diffusion, measured with 2D IR experiments. The small molecule probes all undergo orientational relaxation on multiple time scales that reflect local RTIL structure. Orientational relaxation cannot occur without structural relaxation of the ionic environment around the probes. The relaxation times, which reflect constraint release by the RTIL medium, are affected by factors such as alkyl chain length[32,33] or the amount of water in the RTIL.[69] The small probes all exhibit relatively fast reorientation, although the details of the orientational relaxation differ from one probe to another owing to their different intermolecular interactions with the IL.

One common characteristic of both the orientational relaxation and the spectral diffusion of the small molecule probes is that even the slowest components randomize the orientation and the probe frequency on time scales that are much faster than the complete randomization of the bulk RTIL structure.[26,27,32,33] The time for bulk structural randomization is obtained from OHD-OKE experiments. Fast orientational relaxation of a small probe molecule in a bath of much larger ions may not seem surprising, but the probe orientational relaxation requires structural rearrangement of the surrounding ions. The fast probe reorientation shows that not all degrees of freedom of the IL need to relax to enable the small probe to randomize its orientation. Likewise, the spectral diffusion samples all frequencies much more rapidly than the complete structural randomization of the IL. This fact demonstrates that the inhomogeneous broadening arises from a subset of all structures in the IL. Therefore, the limited subset of structures that produce the inhomogeneous line are sampled quickly compared to all of the structures in the liquid. This leads to an important conclusion: The small probes report on a subset of structures and interactions that influence them, which do not span all of the structures in the IL.

To go beyond small-molecule probes of RTILs, we synthesized a vibrational probe that is based on the cation of the IL. BmimNTf$_2$ was studied using 2-SeCN-Bmim$^+$ by probing the CN stretch of the SeCN moiety. Orientational relaxation measurements gave two components of fast relaxation that like the small-molecule probes were attributed to angular motion over limited ranges, that is, wobbling-in-a-cone. The time constants for the wobbling processes were quite similar to those of the small anion, SeCN$^-$, showing that these wobbling motions involve relaxation of a limited set of IL structures. However, in contrast to the small-molecule probes, the final diffusive orientational randomization occurred with the same time constant as the orientational randomization of the bulk liquid measured with the OHD-OKE experiment.

In BmimNTf$_2$, the inhomogeneous line width of 2-SeCN-Bmim$^+$ is greater than that of SeCN$^-$. Whereas more local variations in structure completely determine the inhomogeneous broadening of small anionic and neutral solutes, a major

DOI: 10.1021/jacs.6b12011
J. Am. Chem. Soc. 2017, 139, 2408−2420

contribution to the inhomogeneous line shape of 2-SeCN-Bmim$^+$ is an additional component. The final spectral diffusion component of 2-SeCN-Bmim$^+$ is on the same time scale as the complete structural randomization of the bulk liquid, while the faster components are almost the same as the time scales of the small probe SeCN$^-$ (Table 4). The results show that the 2-SeCN-Bmim$^+$ vibrational line is influenced by all of the structural degrees of freedom of the IL, in contrast to the small molecule probes that are influenced only by a subset of all structures. Therefore, 2-SeCN-Bmim$^+$, being very similar to the native cation, provides a global perspective on the dynamics and interactions in the IL.

■ ASSOCIATED CONTENT

Supporting Information

The Supporting Information is available free of charge on the ACS Publications website at DOI: 10.1021/jacs.6b12011.

Synthesis and characterization of 2-selenocyanate-1-butyl-3-methylimidazolium bis(trifluoromethylsulfonyl)-imide, characterization of 1-butyl-3-methylimidazolium selenocyanate, wobbling-in-a-cone model of orientational relaxation, hydrodynamic calculation of 2-SeCN-Bmim$^+$ diffusive orientational relaxation time, data figures and tables (PDF)

■ AUTHOR INFORMATION

Corresponding Author

*Phone: (650) 723-4446. E-mail: fayer@stanford.edu.

ORCID

Amr Tamimi: 0000-0001-6873-4471

Michael D. Fayer: 0000-0002-0021-1815

Present Addresses

C.L.: College of Chemistry and Materials Science, South Central University for Nationalities, Wuhan, Hubei, PR China. A.T.: Department of Chemistry and Biochemistry, University of Oregon Eugene, OR 97403, USA.

Notes

The authors declare no competing financial interest.

■ ACKNOWLEDGMENTS

This work was funded by the Division of Chemical Sciences, Geosciences, and Biosciences, Office of Basic Energy Sciences of the U.S. Department of Energy through Grant no. DE-FG03-84ER13251 (S.A.Y., A.T., and M.D.F.). The Division of Chemistry, Directorate of Mathematical and Physical Sciences National Science Foundation (NSF) (CHE-1461477) provided support for the OHD-OKE instrumentation and for H.E.B and M.D.F. Additional support of the 2D IR instrument and for M.D.F. was provided by the Air Force Office of Scientific Research grant number FA9550-16-1-0104. A.T. acknowledges support from a Stanford Graduate Fellowship.

■ REFERENCES

(1) Armand, M.; Endres, F.; MacFarlane, D. R.; Ohno, H.; Scrosati, B. *Nat. Mater.* **2009**, *8*, 621.

(2) Castner, E. W., Jr.; Margulis, C. J.; Maroncelli, M.; Wishart, J. F. *Annu. Rev. Phys. Chem.* **2011**, *62*, 85.

(3) Hayes, R.; Warr, G. G.; Atkin, R. *Chem. Rev.* **2015**, *115*, 6357.

(4) Galiński, M.; Lewandowski, A.; Stępniak, I. *Electrochim. Acta* **2006**, *51*, 5567.

(5) Lewandowski, A.; Świderska-Mocek, A. *J. Power Sources* **2009**, *194*, 601.

(6) Cadena, C.; Anthony, J. L.; Shah, J. K.; Morrow, T. I.; Brennecke, J. F.; Maginn, E. J. *J. Am. Chem. Soc.* **2004**, *126*, 5300.

(7) Kosan, B.; Michels, C.; Meister, F. *Cellulose* **2008**, *15*, 59.

(8) Wang, Y.; Voth, G. A. *J. Am. Chem. Soc.* **2005**, *127*, 12192.

(9) Canongia Lopes, J. N. A.; Pádua, A. A. H. *J. Phys. Chem. B* **2006**, *110*, 3330.

(10) Russina, O.; Triolo, A.; Gontrani, L.; Caminiti, R.; Xiao, D.; Hines, L. G., Jr.; Bartsch, R. A.; Quitevis, E. L.; Plechkova, N.; Seddon, K. R. *J. Phys.: Condens. Matter* **2009**, *21*, 424121.

(11) Rocha, M. A. A.; Lima, C. F. R. A. C.; Gomes, L. R.; Schröder, B.; Coutinho, J. A. P.; Marrucho, I. M.; Esperança, J. M. S. S.; Rebelo, L. P. N.; Shimizu, K.; Lopes, J. N. C.; Santos, L. M. N. B. F. *J. Phys. Chem. B* **2011**, *115*, 10919.

(12) Rocha, M. A. A.; Bastos, M.; Coutinho, J. A. P.; Santos, L. M. N. B. F. *J. Chem. Thermodyn.* **2012**, *53*, 140.

(13) Rocha, M. A. A.; Neves, C. M. S. S.; Freire, M. G.; Russina, O.; Triolo, A.; Coutinho, J. A. P.; Santos, L. M. N. B. F. *J. Phys. Chem. B* **2013**, *117*, 10889.

(14) Annapureddy, H. V. R.; Kashyap, H. K.; De Biase, P. M.; Margulis, C. J. *J. Phys. Chem. B* **2010**, *114*, 16838.

(15) Shimizu, K.; Bernardes, C. E. S.; Canongia Lopes, J. N. *J. Phys. Chem. B* **2014**, *118*, 567.

(16) Nicolau, B. G.; Sturlaugson, A.; Fruchey, K.; Ribeiro, M. C. C.; Fayer, M. D. *J. Phys. Chem. B* **2010**, *114*, 8350.

(17) Sturlaugson, A. L.; Arima, A. Y.; Bailey, H. E.; Fayer, M. D. *J. Phys. Chem. B* **2013**, *117*, 14775.

(18) Sturlaugson, A. L.; Fruchey, K. S.; Fayer, M. D. *J. Phys. Chem. B* **2012**, *116*, 1777.

(19) Yang, P.; Voth, G. A.; Xiao, D.; Hines, L. G.; Bartsch, R. A.; Quitevis, E. L. *J. Chem. Phys.* **2011**, *135*, 034502.

(20) Fruchey, K.; Fayer, M. D. *J. Phys. Chem. B* **2010**, *114*, 2840.

(21) Lawler, C.; Fayer, M. D. *J. Phys. Chem. B* **2013**, *117*, 9768.

(22) Wu, B.; Liang, M.; Maroncelli, M.; Castner, E. W., Jr. *J. Phys. Chem. B* **2015**, *119*, 14790.

(23) Zhang, X.-X.; Breffke, J.; Ernsting, N. P.; Maroncelli, M. *Phys. Chem. Chem. Phys.* **2015**, *17*, 12949.

(24) Wong, D. B.; Giammanco, C. H.; Fenn, E. E.; Fayer, M. D. *J. Phys. Chem. B* **2013**, *117*, 623.

(25) Ren, Z.; Ivanova, A. S.; Couchot-Vore, D.; Garrett-Roe, S. *J. Phys. Chem. Lett.* **2014**, *5*, 1541.

(26) Ren, Z.; Brinzer, T.; Dutta, S.; Garrett-Roe, S. *J. Phys. Chem. B* **2015**, *119*, 4699.

(27) Kramer, P. L.; Giammanco, C. H.; Fayer, M. D. *J. Chem. Phys.* **2015**, *142*, 212408.

(28) Kramer, P. L.; Nishida, J.; Giammanco, C. H.; Tamimi, A.; Fayer, M. D. *J. Chem. Phys.* **2015**, *142*, 184505.

(29) Giammanco, C. H.; Kramer, P. L.; Yamada, S. A.; Nishida, J.; Tamimi, A.; Fayer, M. D. *J. Phys. Chem. B* **2016**, *120*, 549.

(30) Giammanco, C. H.; Kramer, P. L.; Yamada, S. A.; Nishida, J.; Tamimi, A.; Fayer, M. D. *J. Chem. Phys.* **2016**, *144*, 104506.

(31) Tamimi, A.; Fayer, M. D. *J. Phys. Chem. B* **2016**, *120*, 5842.

(32) Giammanco, C. H.; Yamada, S. A.; Kramer, P. L.; Tamimi, A.; Fayer, M. D. *J. Phys. Chem. B* **2016**, *120*, 6698.

(33) Tamimi, A.; Bailey, H. E.; Fayer, M. D. *J. Phys. Chem. B* **2016**, *120*, 7488.

(34) Brinzer, T.; Berquist, E. J.; Ren, Z.; Dutta, S.; Johnson, C. A.; Krisher, C. S.; Lambrecht, D. S.; Garrett-Roe, S. *J. Chem. Phys.* **2015**, *142*, 212425.

(35) Park, S.; Kwak, K.; Fayer, M. D. *Laser Phys. Lett.* **2007**, *4*, 704.

(36) Solangi, A.; Bond, A. M.; Burgar, I.; Hollenkamp, A. F.; Horne, M. D.; Rüther, T.; Zhao, C. *J. Phys. Chem. B* **2011**, *115*, 6843.

(37) Karthick Kumar, S. K.; Tamimi, A.; Fayer, M. D. *J. Chem. Phys.* **2012**, *137*, 184201.

(38) Shim, S.-H.; Strasfeld, D. B.; Fulmer, E. C.; Zanni, M. T. *Opt. Lett.* **2006**, *31*, 838.

(39) Shim, S.-H.; Zanni, M. T. *Phys. Chem. Chem. Phys.* **2009**, *11*, 748.

(40) Tokmakoff, A. *J. Chem. Phys.* **1996**, *105*, 1.

DOI: 10.1021/jacs.6b12011
J. Am. Chem. Soc. 2017, 139, 2408−2420

(41) Tan, H.-S.; Piletic, I. R.; Fayer, M. D. *J. Opt. Soc. Am. B* **2005**, *22*, 2009.
(42) Hamm, P.; Zanni, M. T. *Concepts and Methods of 2D Infrared Spectroscopy*; Cambridge University Press: New York, 2011.
(43) Kramer, P. L.; Nishida, J.; Fayer, M. D. *J. Chem. Phys.* **2015**, *143*, 124505.
(44) Nishida, J.; Tamimi, A.; Fei, H.; Pullen, S.; Ott, S.; Cohen, S. M.; Fayer, M. D. *Proc. Natl. Acad. Sci. U. S. A.* **2014**, *111*, 18442.
(45) McMorrow, D.; Lotshaw, W. T.; Kenney-Wallace, G. A. *IEEE J. Quantum Electron.* **1988**, *24*, 443.
(46) Yuan, R.; Yan, C.; Tamimi, A.; Fayer, M. D. *J. Phys. Chem. B* **2015**, *119*, 13407.
(47) Tao, T. *Biopolymers* **1969**, *8*, 609.
(48) Del Pópolo, M. G.; Voth, G. A. *J. Phys. Chem. B* **2004**, *108*, 1744.
(49) Lipari, G.; Szabo, A. *Biophys. J.* **1980**, *30*, 489.
(50) Tan, H.-S.; Piletic, I. R.; Fayer, M. D. *J. Chem. Phys.* **2005**, *122*, 174501.
(51) Kinosita, K.; Kawato, S.; Ikegami, A. *Biophys. J.* **1977**, *20*, 289.
(52) Lipari, G.; Szabo, A. *J. Am. Chem. Soc.* **1982**, *104*, 4546.
(53) Urahata, S. M.; Ribeiro, M. C. C. *J. Chem. Phys.* **2005**, *122*, 024511.
(54) Hazelbaker, E. D.; Budhathoki, S.; Katihar, A.; Shah, J. K.; Maginn, E. J.; Vasenkov, S. *J. Phys. Chem. B* **2012**, *116*, 9141.
(55) Sha, M.; Dong, H.; Luo, F.; Tang, Z.; Zhu, G.; Wu, G. *J. Phys. Chem. Lett.* **2015**, *6*, 3713.
(56) Moog, R. S.; Ediger, M. D.; Boxer, S. G.; Fayer, M. D. *J. Phys. Chem.* **1982**, *86*, 4694.
(57) Youngren, G. K.; Acrivos, A. *J. Chem. Phys.* **1975**, *63*, 3846.
(58) Sension, R. J.; Hochstrasser, R. M. *J. Chem. Phys.* **1993**, *98*, 2490.
(59) Hu, C. M.; Zwanzig, R. *J. Chem. Phys.* **1974**, *60*, 4354.
(60) Kwak, K.; Park, S.; Finkelstein, I. J.; Fayer, M. D. *J. Chem. Phys.* **2007**, *127*, 124503.
(61) Kwak, K.; Rosenfeld, D. E.; Fayer, M. D. *J. Chem. Phys.* **2008**, *128*, 204505.
(62) Akaike, H. *IEEE Trans. Autom. Control* **1974**, *19*, 716.
(63) Park, S.; Fayer, M. D. *Proc. Natl. Acad. Sci. U. S. A.* **2007**, *104*, 16731.
(64) Laage, D.; Hynes, J. T. *Science* **2006**, *311*, 832.
(65) Laage, D.; Hynes, J. T. *Proc. Natl. Acad. Sci. U. S. A.* **2007**, *104*, 11167.
(66) Laage, D.; Hynes, J. T. *J. Phys. Chem. B* **2008**, *112*, 14230.
(67) Fecko, C. J.; Eaves, J. D.; Loparo, J. J.; Tokmakoff, A.; Geissler, P. L. *Science* **2003**, *301*, 1698.
(68) Fecko, C. J.; Loparo, J. J.; Roberts, S. T.; Tokmakoff, A. *J. Chem. Phys.* **2005**, *122*, 054506.
(69) Giammanco, C. H.; Kramer, P. L.; Wong, D. B.; Fayer, M. D. *J. Phys. Chem. B* **2016**, *120*, 11523.

DOI: 10.1021/jacs.6b12011
J. Am. Chem. Soc. 2017, 139, 2408−2420